

RESEARCH ARTICLE

WILEY

Impact and mitigation of blade surface roughness effects on wind turbine performance

Jack Kelly  | Christopher Vogel  | Richard Willden

Department of Engineering Science, University of Oxford, Oxford, UK

Correspondence

Jack Kelly, Department of Engineering Science, University of Oxford, Oxford, UK.

Email: jack.kelly@seh.ox.ac.uk

Funding information

EPSRC Advanced Fellowship, Grant/Award Number: EP/R007322/1; EPSRC Supergen ORE Hub, Grant/Award Number: EP/S000747/1

Abstract

This paper presents a numerical study of the effects of blade roughness on wind turbine performance and annual energy production and how these effects may be partially mitigated through improved control. Three rotors are designed using the NACA4415, S801 and S810 airfoils, and blade element momentum theory is used to model wind turbine behaviour. The aerodynamic lift and drag data for the clean and roughened airfoils are taken from previous experimental work. These show that surface roughness leads to a decreased airfoil lift coefficient and an increased drag coefficient across an angle of attack range typical for large wind turbines, which will clearly lead to decreased turbine performance. Three separate control methods are considered for wind turbines with roughened blades operating at each of four candidate wind sites with different wind speed distributions. Results show that, compared to clean rotor blades, the roughened blades lead to a performance drop in the range of 2.9–8.6% for a torque based control strategy. A control-based performance recovery strategy, in which the controller gain coefficient is re-optimised, increased roughened rotor annual energy production by 0.1–1.0%.

KEYWORDS

blade roughness, control strategies, wind power

1 | INTRODUCTION

Wind turbine performance can change as the aerodynamic quality of the blade surface degrades over time. This occurs because wind turbines are exposed to different weather conditions and airborne particles that may damage or alter the rotor's aerodynamic surfaces. This 'roughness' that occurs on rotor blades may arise due to ice accretion, surface erosion, insect damage or other causes which are influenced by turbine location. The impact of roughness on a turbine's annual energy production (AEP) is a combination of the reduction in turbine performance caused by the roughness source(s), predominantly encountered below the turbine's rated power and the wind speed distribution, that is, how likely the turbine is to be operating below the rated power.

Roughness impacts on turbine performance can be significant. Corten and Veldkamp¹ showed in field tests that roughness due to insect contamination can result in power losses of over 25%. Jasinski et al² show that turbine performance can decrease by up to 20%, while Corrigan and DeMiglio³ concluded that heavy rain can degrade performance by as much as 30%. Khalfallah and Koliub⁴ also show power losses between 6.5% and 38% for different diameter dust particles on turbine blades.

This is an open access article under the terms of the Creative Commons Attribution License, which permits use, distribution and reproduction in any medium, provided the original work is properly cited.

© 2021 The Authors. *Wind Energy* published by John Wiley & Sons Ltd.

Turbine power loss from roughness arises from decreased airfoil lift and increased airfoil drag, which results in rotor power loss. Multiple experimental tests have been performed to measure the impact of icing on the aerodynamic performance of an airfoil.^{5–7} Krøgenes and Brandrud⁶ and Hann et al⁷ both investigate the impacts on the NREL S826 airfoil under different icing conditions. Their results were synthesised by Vinnes and Hearst⁸ and showed a 10% decrease in lift and 80% increase in drag. They also showed that a heavily ice affected airfoil reduces the angle of attack stall first occurs, which agrees with results published by DeGregorio et al⁹ who investigated the NACA0012 airfoil under similar ice accretion geometries.

Many studies provide insight into the aerodynamic effects of airfoil roughness,^{10,11} but few investigate the overall effect on wind turbine power performance. Blasco et al⁵ analysed the effect of icing on an airfoil using wind tunnel experimental testing. They used blade element momentum (BEM) software XTurb-PSU¹² to conclude that the changed aerodynamic performance of the airfoil implied a 16–22% reduction in power for a wind turbine in freezing fog conditions and 26% for a freezing drizzle condition. They also showed that modifying the blade pitch controller to start blade pitching at a higher wind speed resulted in greater power production when the blades were roughened.

The availability of roughened airfoil data is limited because roughness is difficult to define and model computationally. The level of mesh detail required to resolve fully the boundary layer developed by the irregular and three-dimensional geometry of airfoil roughness is hard to define and computationally prohibitive. Furthermore, wall-modelling turbulence closures to computational fluid dynamics (CFD) models are unvalidated for roughness applications. A study of simplified surface roughness representations on the NACA 63₃-418 airfoil was undertaken by Krog Kruse et al¹³ using the DTU Wind Energy CFD Reynolds-Averaged Navier–Stokes (RANS) solver, EllipSys2D. An up to 35% reduction in lift and 90% lift-to-drag ratio reduction was found, depending on how extensive the surface imperfections were. Munduate and Ferrer¹⁴ examined the roughness-modelling capability of Xfoil through comparison to CFD analysis. They showed that Xfoil was insufficient for modelling wind turbine blade roughness. They also showed that although airfoil forces can be determined computationally, the transition between laminar and turbulent boundary layer flow, and especially the impact of surface roughness, is difficult to simulate accurately. Consequently, due to the limitations of computational blade flow modelling, experimental blade data are used in the present study.

The literature on the effect of roughness on wind turbine performance predominantly focuses on the impact on the coefficient of performance (C_p) and not AEP. However, Schramm et al¹⁵ use numerical methods to simulate roughness effects on the NREL 5MW reference wind turbine across all wind speeds using CFD methods to evaluate airfoil aerodynamic coefficients which were then used to model the turbine through a BEM model (FAST v8¹⁶). Roughness was represented by deforming the leading edge of the airfoil (to simulate erosion), and the airfoil performance coefficients were determined through RANS CFD simulation with the $k-\omega$ SST model, where a wall roughness function was used. While all operational wind speeds were considered, this approach is limited because turbine control to mitigate the effect of roughness was not part of the investigation.

Similarly, Pechlivanoglou et al¹⁷ used an in-house BEM simulation method based on Hansen¹⁸ to produce a power distribution as a function of wind speed for a 1.5-MW turbine. However, their study was primarily focussed on the effects of roughness on airfoil performance through wind tunnel experiments, and they only provided a limited BEM analysis of the consequences for wind turbine performance. Bak et al¹⁹ investigated the effect of five different roughness types (bumps, erosion, overhang, etc.) using CFD across three different wind climates and different maximum tip speeds. They show AEP losses of 0.5–4% and also that increasing the maximum tip speed (for both clean and rough cases) decreased the magnitude of losses. This is an example of a potential design strategy for a clean rotor to mitigate the effect of roughness when it occurs. A different approach is used in this study, which uses a control strategy to mitigate the effect of roughness regardless of what the design tip speed of the clean rotor is.

Turbine control has the potential to reduce the negative impacts of turbine roughness, either through reducing the likelihood of blade damage occurring in the first place or by adjusting turbine performance once damage has been incurred. Impact damage roughness events such as insect damage and rain can result in permanent damage. However, these events can also be mitigated through the implementation of erosion-safe operation (reducing the tip speed during rain events or insect swarms to minimise impact damage); see Hasager et al.,²⁰ Tilg et al²¹ and Hasager et al.²² Erosion-safe operation has a smaller impact on AEP than permanently damaged blades because the performance losses are only temporary. The focus of this paper is on permanent roughness, and a novel control strategy to mitigate the impact of roughness is proposed.

The aim of this paper is to investigate the potential for turbine control methods to mitigate losses in AEP due to the development of roughness on the blades. The performance of roughened airfoils, tested in research conducted at Ohio State University (OSU) for the National Renewable Energy Laboratory (NREL),²³ is used to model a single wind turbine simulated using BEM methods. The effects of roughness on turbine performance have been explored for three turbines, each designed using a different airfoil profile and exhibiting different aerodynamic characteristics. In all cases, roughness was applied uniformly along the entire span of each rotor blade. Three turbine control strategies have been investigated with an in-house analytic BEM model; two widely adopted in the literature and a novel third control strategy that seeks to mitigate some of the effects of roughness on turbine performance and AEP.

2 | METHOD

2.1 | Computational method and available airfoil tables

The BEM method will be used to examine the effects of roughness on wind turbine performance. The BEM method used for this simulation is a single parameter guaranteed convergence formulation proposed by Ning.²⁴

Prandtl's tip-loss model²⁵ is included to account for the influence of discrete and 3-D blade effects that cause a spanwise variation in blade loads and is not directly modelled in the 2-D momentum and blade element equations used in BEM theory. Buhl's thrust correction²⁶ for the turbulent wake state that couples momentum theory with Glauert's empirical model for heavily loaded turbines with hub and tip losses is also included. The model has been validated with reference to previous BEM theory-based models, for example, Vogel et al.²⁷

Although steady wind turbine operation generally corresponds to modest angles of attack along most of the blade span (0–10°), good numerical convergence of the BEM model requires smooth and continuous lift and drag data over a much wider range of angle of attack (α). Some processing of experimental data is inevitably required to achieve this.

Airfoil aerodynamic characteristics (lift, drag) must be specified in order to use a BEM simulation for wind turbine performance. Airfoil data for both aerodynamically smooth and rough conditions were used in this study. Experimental data published by OSU researchers under contract from the NREL²³ are used in this study. The data were collected using wind tunnel experiments to determine the lift and drag profiles of specific airfoils.²⁸ Lift and drag forces are converted to non-dimensional parameters, the sectional lift and drag coefficients, c_l and c_d respectively.

The advantage of using airfoil data from one study is that an equivalent level of roughness is applied in each test. A standard roughness pattern was developed from a moulded insect pattern taken from a wind turbine in the field¹⁰ and used for all airfoils. To simulate leading edge accumulation of roughness, the density of roughness particles ranged from 5 particles per cm² in the centre of the pattern to 1.25 particles per cm² at the edge. Based on average particle size from the field specimen, the non-dimensional roughness height was $k/c = 0.0019$ where k is the roughness height and c is the blade chord length.¹⁰

Wind tunnel testing was conducted for 13 airfoils (L303, LS417, LS421, NACA4415, S801, S809, S810, S812, S813, S814, S815, S824 and S825). All airfoils were tested in the OSU Aeronautical and Astronautical Research Laboratory (AARL) 3 × 5 foot subsonic wind tunnel under steady flow conditions.¹⁰ Data were acquired and processed from 60 surface pressure taps, four individual tunnel pressure transducers, an angle of attack potentiometer, a wake probe position potentiometer and a tunnel thermocouple.¹⁰ The results and data from these tests are publicly available,²³ and these data have also been used for other airfoil roughness CFD studies by Munduate and Ferrer.¹⁴

The OSU/NREL wind tunnel experiments were conducted across a range of chord-based Reynolds numbers (Re) (0.75 to 1.5 million) for each airfoil. Reynolds number is defined as the ratio of inertial forces to viscous forces within a fluid. Only the data from the highest Re experiment were used in the present study (1.25 or 1.5 million depending on the airfoil) as the airfoil boundary layer flow is expected to be post-transitional and therefore most representative of a utility-scale wind turbine.

The range of drag data needed to be extrapolated because drag measurements only occurred at low angle of attack values (approximately –10° to 10°). This is because the drag value was calculated from pressure measurements in the wake and could not be accurately calculated when there was a lot of turbulence as arises in separated flow at high angles of attack.²⁹ Consequently, the lowest and highest recorded angles of attack were uniformly extended beyond this angle of attack range. This simplistic approximation, required to ensure convergence of the BEM model, did not affect the final predicted rotor performance in the conditions simulated in this study.

2.1.1 | Airfoil selection

The three airfoils listed in Table 1 were chosen to be analysed based on three factors: $(c_l/c_d)^*$ for both the clean and rough airfoils as well as the difference in magnitude of these values; the corresponding change in α^* between the clean and rough airfoils; and the shape of the c_l/c_d versus α graph. A large lift to drag ratio is desired to maximise torque production and thus achieve efficient turbine operation. The optimal angle of attack value, α^* , and the c_l/c_d versus α curve are important because a rotor designed to operate at α_{clean}^* could operate significantly away from $(c_l/c_d)_{rough}^*$ when the airfoil transitions from smooth to rough conditions. This has the potential to exacerbate the performance decline in roughened conditions due to the combined effects of roughness reducing the c_l/c_d ratio and operating away from the maximum c_l/c_d condition. Figure 1 shows c_l/c_d versus α as well as the aerodynamic polars for the NACA4415, S801 and S810 airfoils under clean and rough conditions. Note that the vertical bars (constant c_d) are present in the c_l/c_d polars due to the extrapolation of the final drag measurement to higher magnitude angle of attack values.

The chosen airfoils all had high clean airfoil $(c_l/c_d)^*$ values with differing α^* positions and differing c_l/c_d versus α characteristics (broadness of lift-to-drag peak). It was postulated that these differences would give insight into the performance differences experienced by different types of rotor as their airfoils transition from clean to rough.

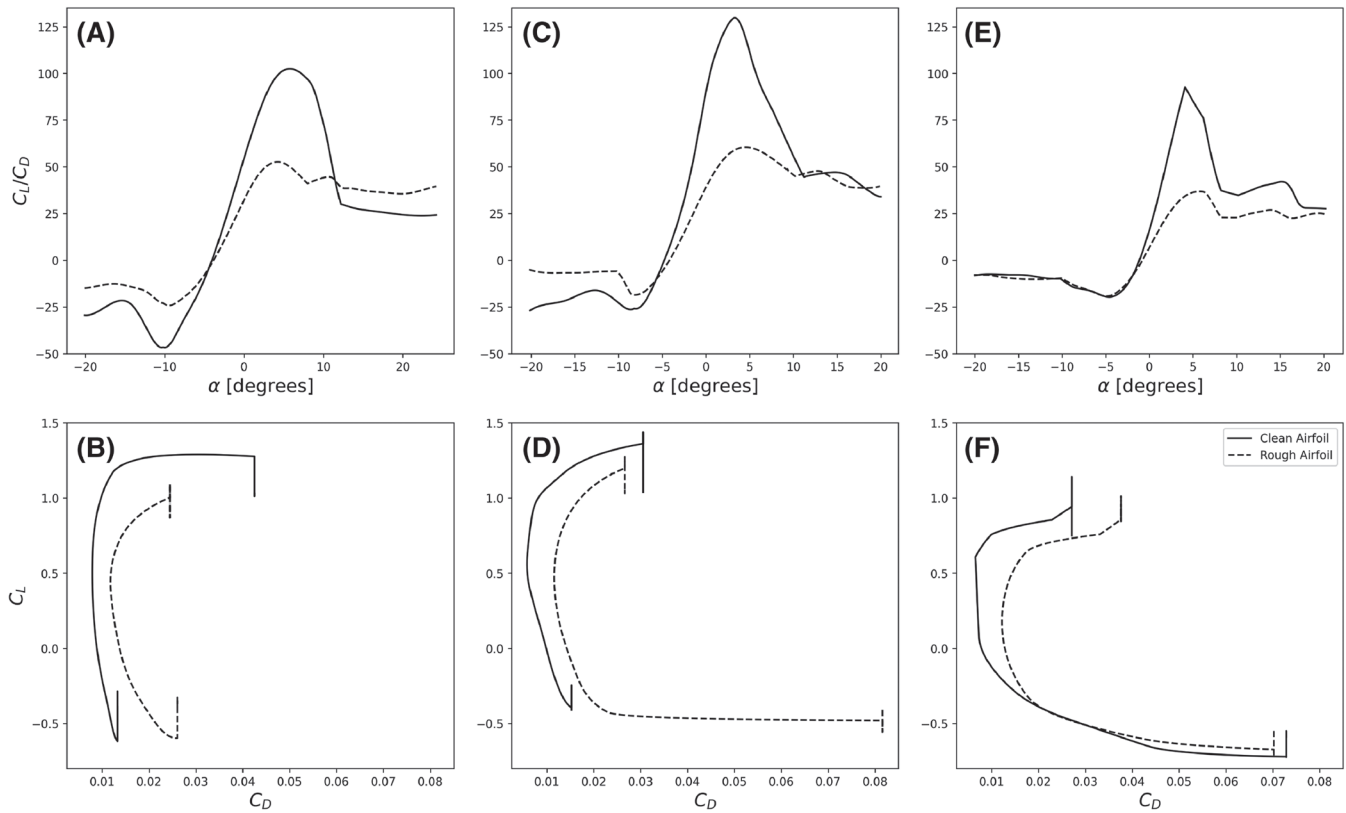


FIGURE 1 Lift to drag ratio and aerodynamic polars for the three selected airfoils (NACA4415, S801, S810). Plots (A) and (B) present the NACA4415 airfoil data, (C) and (D) present the S801 airfoil and (E) and (F) present the S810 airfoil

TABLE 1 Summary of maximum lift to drag ratio and corresponding angle of attack and chord-based Reynolds number for three selected airfoils from the OSU study²⁸

Airfoil	Condition	$(C_L/C_D)^*$	α^* [degrees]	$C_{L,max}$	α range [degrees]	$Re \times 10^6$
NACA4415	Clean	102.45	5.8	1.29	−10.2 to 12.2	1.5
NACA4415	Rough	52.64	4.2	1.09	−10.2 to 8	1.5
S801	Clean	129.75	3.3	1.44	−8.2 to 11.2	1.5
S801	Rough	60.50	4.5	1.27	−10.2 to 10.2	1.5
S810	Clean	92.62	4.1	1.14	−10.2 to 10.2	1.5
S810	Rough	36.84	5.8	1.01	−10.1 to 10.1	1.5

The S801 and S810 airfoils were designed for use on small wind turbines (20–400 kW) and to be resistant to leading edge erosion.³⁰ They were designed to have a $C_{L,max}$ which is largely insensitive to roughness (as shown in Table 1); however, C_D may still increase significantly. These airfoils were designed to have laminar to turbulent transition on the suction surface occur close to the leading edge just prior to reaching $C_{L,max}$. We do not expect this to significantly change at higher chord-based Reynolds number. Using these airfoils on larger rotors may not be as representative of airfoils used on utility scale turbines but do allow for a data-driven approach to analyse the effect of roughness. For more details on the original experimental studies completed on these airfoils, see Hoffman et al.,²⁹ Reuss Ramsay et al.³¹ and Reuss Ramsay et al.³²

2.2 | Rotor design

Three rotors were designed to investigate the effects of roughness on turbine performance given the different characteristics of the selected airfoils. For simplicity in evaluating the impact of airfoil roughness on turbine performance, a constant airfoil profile was used throughout the span of each rotor's blades. A conventional variable-speed, variable blade pitch-to-feather configuration wind turbine was assumed, and the rotors were designed to meet the following parameters:

- Design Tip Speed Ratio $\lambda^* = 10$; $\lambda = R\omega/U$, where ω is the rotational speed of the turbine and U is wind speed.
- Maximum rotational speed $\omega_r = 2$ rad/s
- Diameter = 100 m
- Hub Radius = 5 m
- Cut-in wind speed $U_{ci} = 3$ m/s
- Rated wind speed $U_r = 10$ m/s
- Cut-out wind speed $U_{co} = 20$ m/s
- Approximate rated power $P_r \approx 2.4$ MW
- Design coefficient of performance $C_p^* \approx 0.5$; $C_p = P/((1/2)\rho U^3 A)$.

C_p is the power coefficient and is ratio of the shaft power generated to the kinetic energy flux of the undisturbed flow through the rotor plane, ρ is the air density and A the turbine swept area. These parameters are chosen to be representative of the size and performance of wind turbines that are currently in the field. Current similar sized commercial offerings include the Vestas V120-2.2 MW³³ and Siemens SG 2.6-114.³⁴

Two planform parameters were used to characterise the rotor blade design: blade twist distribution and chord length distribution. These were set via an iterative BEM solution in which the rotor is divided into a number of concentric annular elements. The blade twist distribution was set such that the angle of attack was equal to α^* for the clean airfoil along the blade, thereby approximately maximising torque production with the airfoils in the clean state. The chord distribution was determined by setting a target local thrust coefficient of $C_x = 2.0$ along the entire length of each blade, which corresponds to the optimal local thrust coefficient from Betz theory for the optimal rotor in an unbounded flow. The local thrust coefficient is defined as

$$C_x = \frac{\delta F_x}{(1/2)\rho U_x^2 \delta A} \quad (1)$$

where δF_x is the streamwise force on a corresponding annular element of area δA and U_x is the streamwise wind velocity at the rotor plane for that annular element.

The rotor solidity ($\sigma_r = Bc/2\pi r$, where B is the number of blades and c is the local chord) and twist (γ) of the rotor designs is shown in Figure 2. We do not modify the inboard taper of the blade due to the focus of this paper on the aerodynamics, rather than on the practical structural requirements, of blade design. Consequently, the sectional Reynolds number is approximately constant along the blade span due to the contrasting effects of increasing incidence velocity and reducing chord length as functions of radius. It should be noted that near the hub, the solidity is relatively large and would usually be replaced by thicker airfoils and a cylindrical section to provide the necessary structure to support the rotor blades. However, the focus of this study is on the impact of airfoil roughness on rotor performance, and hence, a single airfoil cross-section is used for the entire blade span to simplify the following analysis. Relatively little torque and therefore power is generated near the blade root so this simplification is considered unlikely to significantly alter the conclusions of this roughness study.

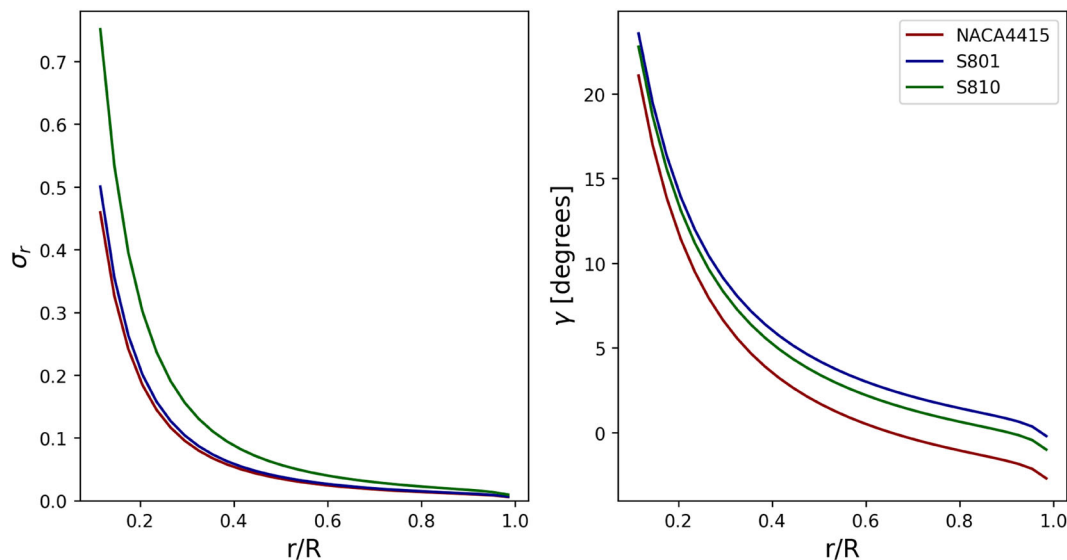


FIGURE 2 Spanwise distribution of rotor solidity σ_r (left) and blade twist angle γ (right) for rotor designs using the NACA4415 (red), S801 (blue) and S810 (green) airfoils

2.3 | Turbine control

Rotor performance loss was evaluated by comparing turbine performance with the clean and roughened airfoils. For the roughened case, the roughened airfoil data were applied along the entire blade span, implying a uniform roughness distribution. This is clearly an approximation, and it is known that blades tend to roughen more rapidly towards the blade tips where they experience higher impact velocities. Alternative roughness distributions may be more representative than this first-order approximation and will be the subject of future studies. The completely roughened blade assumption is however useful as it provides an upper bound on the detrimental effects of blade roughness.

The reduced lift and increased drag that arises as roughness develops results in a reduction in rotor torque and thus power at a given wind speed. Consequently, higher wind speeds or higher turbine rotational speeds are required to recover the torque to the levels observed with clean airfoil conditions. The reduction in torque interacts non-linearly with rotor control mechanisms, which may act to modify the behaviour of the rotor and therefore impact on turbine performance.

Turbine performance was evaluated across the full range of wind speeds from cut-in to cut-out to assess the impact of roughness on overall energy production. It is assumed that turbine control is based only on the following data:

- Rotational speed of the rotor (ω)
- Root pitch setting angle of the blades (β)
- Generator torque (τ_{gen})

The generator torque, τ_{gen} , can be different to the expected aerodynamic torque on the rotor blades (τ_{aero}), which, in the present analysis, is determined through a BEM solution. This is an important distinction as generator torque can in practice be directly measured, whereas the aerodynamic torque is inferred.³⁵

These control parameters are the same as those chosen to control the NREL 5MW reference turbine.³⁶ The NREL turbine operates using two control systems: a generator-torque controller and a full-span collective blade-pitch controller. The two control systems work independently, for the most part, in the below-rated and above-rated wind speed ranges, respectively. The goal of the generator-torque controller is to maximise power capture below the rated operation point, and the goal of the blade-pitch controller is to regulate generator speed and rotor torque above this point. The transition from below- to above-rated flow speed control systems typically starts from around 1 m/s below the rated flow speed. For simplicity, the transition between rotor control below and above rated flow speed is neglected herein, but this simplification is not expected to significantly alter the conclusions of this study.

Two control paradigms were considered in the present work: referencing turbine control to the rotational speed ω ; and referencing turbine control to generator torque τ_{gen} . The blade-pitch controller was employed above the rated flow speed in both cases. An optimised generator torque method was also investigated, and the methodology for each is explained below. For all simulations, it was assumed that the ‘cut-in’ torque was equal to the torque generated by the rotor with clean airfoil blades at the cut-in wind speed (3 m/s).

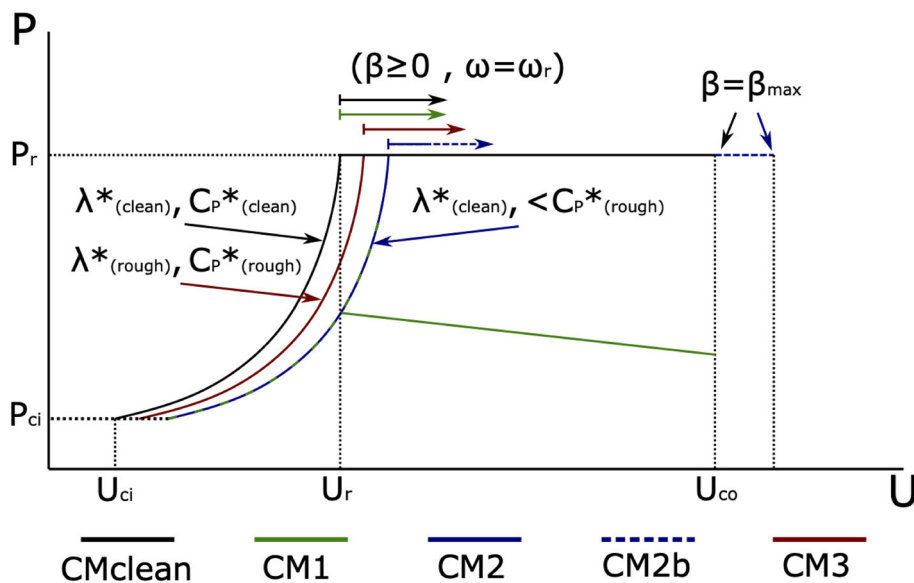


FIGURE 3 Schematic of the different control strategies used for both clean and rough rotors. All control methods with a clean blade yield identical power curves and have been labelled “CMclean”

Figure 3 shows a schematic power-wind speed plot for all control methods and is presented to aid the explanation of the control methods. To do this, a clean and rough operation curve is shown for each control method, with exaggerated differences to highlight changes. All control methods with a clean blade yield identical power curves and are simply labelled 'CMclean'. The control methods are outlined below and an overview provided in Table 2.

2.3.1 | CM1: Wind speed referenced

A reference case was established in which the turbine rotational speed and blade pitch angle are varied at the same rate with the flow speed as in the clean turbine case. In reality, this would require the wind speed to be measured and the turbine control to be based solely off of this in a prescribed manner rather than being controlled in response to observed generator torque. This is consistent with existing power-wind speed control paradigms.³⁷ In control method 1 (CM1), the tip speed ratio λ is set to $\lambda^* = 10$ between the cut-in and rated flow speeds, and the rotor performs suboptimally and below the performance level attainable for the roughened rotor, that is, $C_p < C_{p,rough}^*$. Once the rated flow speed is reached, $\omega = \omega_r$, and the blade pitch angle β increases with flow speed at the same rate as in the clean turbine case. The turbine shuts down at the cut-out flow speed U_{co} .

As the rotor torque is reduced by the influence of roughness from the clean case, the maximum torque achieved with this method is less than that at rated conditions for the clean rotor ($\tau_{max} < \tau_r$), and thus, maximum rotor power is necessarily less than the rated power ($P_{max} < P_r$). As the rough rotor follows the pitch profile of the clean rotor, it is likely that $\partial P / \partial U < 0$ beyond rated.

2.3.2 | CM2: Generator torque referenced

Control method 2 (CM2) is an optimal torque control (OTC) technique that is the standard Maximum Power Point Tracking (MPPT) algorithm that is implemented in commercial wind turbines.³⁸ OTC is favoured in this study over other MPPT techniques such as hill-climb search (HCS) and sliding mode control (SMC) because of its popularity in commercial wind turbines and the steady-state nature of BEM which does not allow for control responses to unsteady events such as turbulent flow.

In CM2, below rated flow speed, the generator torque is brought into balance with the aerodynamic torque in steady-state to achieve the following:

$$\tau_{gen} = \tau_{aero} \quad (2)$$

Note that this is not the case during transient or flow speed-varying operation, and it is the equalisation of these torques that is sought through adjustment of rotor speed or collective pitch. The above equilibrium condition yields the following relationship:

$$\tau_{gen} = \left(\frac{1}{2} \rho \pi R^5 \frac{C_p^*}{\lambda^{*3}} \right) \omega^2 = K \omega^2 \quad (3)$$

TABLE 2 Overview of control methods

Control method	$U < U_r$		$U > U_r$		Notes
	Target	Control parameter	Target	Control parameter	
CM1	$\lambda = \lambda_{clean}^*$	$\omega(U)$	$\omega = \omega_r$	$\beta(U)$	Pitching starts at ω_r . Clean pitch followed for both cases.
CM2	$\lambda = \lambda_{clean}^*$	τ_{gen}	$\tau_{gen} = \tau_r$	β	Pitching starts at $\tau_{gen} = \tau_r$. Cut out speed enforced at 20m/s.
CM2b	$\lambda = \lambda_{clean}^*$	τ_{gen}	$\tau_{gen} = \tau_r$	β	Pitching starts at $\tau_{gen} = \tau_r$. Cut out speed enforced at β_{max} .
CM3	$\lambda = \lambda_{rough}^*$	τ_{gen}, K	$\tau_{gen} = \tau_r$	β	K optimised for $\tau_{gen} < \tau_r$. Pitching starts at $\tau_{gen} = \tau_r$. Cut out speed enforced at β_{max} .

where C_p^* and λ^* are defined by the optimal operation point of the turbine. K is the generator torque constant that is predetermined for the case of clean blades (K_{clean}). If the turbine performs such that it generates a power coefficient C_p^* at λ^* , then the controller (Equation 3) works to adjust the rotor's speed in response to changes in the generator torque which is matched to the aerodynamic torque experienced by the rotor (or computed via BEM as in the current analysis).

In CM2, the rotor underperforms relative to the clean condition with $C_p < C_{p_{clean}}^*$ and so the aerodynamic torque is less than expected at any given flow speed below rated, and the rotational speed, set via Equation (3), climbs more slowly. Consequently, in CM2, rated power is reached at a higher flow speed than in the clean condition. When a high enough flow speed is reached so that $\omega = \omega_r$, blade pitching commences to limit generator torque so that $\tau_{gen} = \tau_r$. This occurs at a higher flow speed than in the clean case, but once $\omega = \omega_r$ power yield is unaffected and $P = P_r$ until the cut-out flow speed is reached, at which point the rotor shuts down.

2.3.3 | CM2b: Generator torque referenced with full pitch

Control method 2b (CM2b) is similar to CM2, except that the turbine shuts down when, under conditions of above rated operation and maximum torque, that is, $\tau_{gen} = \tau_r$, maximum blade pitch angle, $\beta = \beta_{max}$, is reached. This means that the rotor will continue operating to wind speeds slightly higher than U_{co} due to the lower blade pitch angle required at any given wind speed above rated in the roughened case.

2.3.4 | CM3: K-optimised torque

The third control method uses the generator constant K as an additional degree of freedom to improve turbine performance. Adjusting K to account for roughness effects enables the controller to modify the rotor's operation to maximise rotor efficiency. A roughness optimised K value, K_{rough} , was found by seeking to maximise AEP, as described below.

By adjusting K for roughness, the turbine will seek to operate at the maximum power coefficient achievable with roughened blades $C_{p(rough)}^*$. This will exceed the power coefficient that would be achieved without adjusting the controller for roughness, and hence, the power curve rises faster with flow speed for control method 3 (CM3) than for CM2 (unadjusted controller with rough blades) but slower than for CMclean (clean blades).

Rated power is reached at a higher flow speed than with clean blades but before it would be reached without adjusting the controller. This control method should therefore present a net energy yield benefit, relative to CM2, as more time is spent at rated flow speed and higher power is delivered below rated than would be achieved without controller adjustment.

Once rated power is achieved, the rotor blades are again pitched to limit the generator torque to $\tau_{gen} = \tau_r$. Blade pitching continues until the maximum permitted pitch is reached at $\beta = \beta_{max}$, resulting in the cut-out flow speed being slightly in excess of that seen in clean conditions, U_{co} .

2.4 | Performance loss

The impact of airfoil roughness on turbine AEP depends not only on the impact on turbine performance (efficiency) but also on the proportion of time that the turbine operates at wind speeds where performance loss is significant. AEP was assessed through numerical integration of Equation (4), where T is the time period (1 year), $P(U)$ represents the power as a function of wind speed and $f(U)$ represents the likelihood of a wind speed U occurring at a particular site.

$$E = T \int_{U_{ci}}^{U_{co}} P(U) f(U) dU \quad (4)$$

The wind speed distribution $f(U)$ is evaluated using a Weibull distribution:³⁹

$$f(U; k_s, c_s) = \frac{k_s}{c_s} \left(\left(\frac{U}{c_s} \right)^{k_s - 1} \right) \exp \left(- \left(\frac{U}{c_s} \right)^{k_s} \right) \quad (5)$$

where k_s is the unitless shape parameter and c_s is the scale parameter in m/s.

Wind speed data from four offshore wind farm sites in the United Kingdom with different flow speed distribution characteristics were investigated: the Kentish Flats, Thanet, Greater Gabbard and Gwynt y Mor. All data were retrieved from the Crown Estate's marine data exchange⁴⁰ and were extrapolated to a common height of 80 m using the log law.⁴¹

$$U(z) = \frac{U_f}{\kappa} \ln\left(\frac{z}{z_0}\right) \quad (6)$$

where U_f is the friction velocity, κ is von Kármán's constant (taken to be 0.4), z is the height at which the velocity is evaluated (here 80 m) and z_0 is the roughness height, which is the height at which the flow speed in the log law profile approaches zero (assumed to be 0.0002 m based off the Davenport terrain roughness classification⁴²). Important data for each of these sites can be found in Table 3.

The wind speed data, available as 10-min average wind speeds through the durations noted in Table 3, were used to determine best fit Weibull wind speed distributions. The determined Weibull shape parameters and scale factors were evaluated and are presented in Table 3. The proportions of the distributions relative to U_{ci} , U_r and U_{co} are given in Table 3 and shown in Figure 4. Differences in these proportions will be important as different wind distributions will affect AEP by changing how much time the turbine spends in pre-rated, post-rated or non-operational regimes. However, the underlying aerodynamic mechanisms causing performance drop will not be considered to be affected by site location.

3 | RESULTS

3.1 | Rotor performance

The rotor designs were simulated with their respective clean and rough airfoil data to evaluate the effects of roughness on overall performance. A summary of the power and thrust coefficients, C_p and C_T , for each rotor operating under rotor design conditions ($\lambda^* = 10$, $U_r = 10$ m/s) for both

TABLE 3 Summary of the four wind sites considered for performance analysis

Site name	Years of data	Original altitude	k_s	c_s [m/s]	$U_{ci} < U < U_r$	$U_r < U < U_{co}$	$U < U_{ci}$ or $U > U_{co}$
Kentish Flats	2002–2005	80 m	2.1073	8.8928	64.6%	27.6%	7.8%
Thanet	2005–2006	10 m	2.3471	9.9750	57.8%	35.7%	6.5%
Greater Gabbard	2005–2014	86 m	2.3028	10.5542	52.3%	40.7%	7.0%
Gwynt y Mor	2005–2007	85 m	2.0306	10.3791	51.0%	39.2%	9.8%

Note: Flow speeds have been extrapolated from data collected at the 'original altitude' through a log law profile to a common altitude of 80 m.

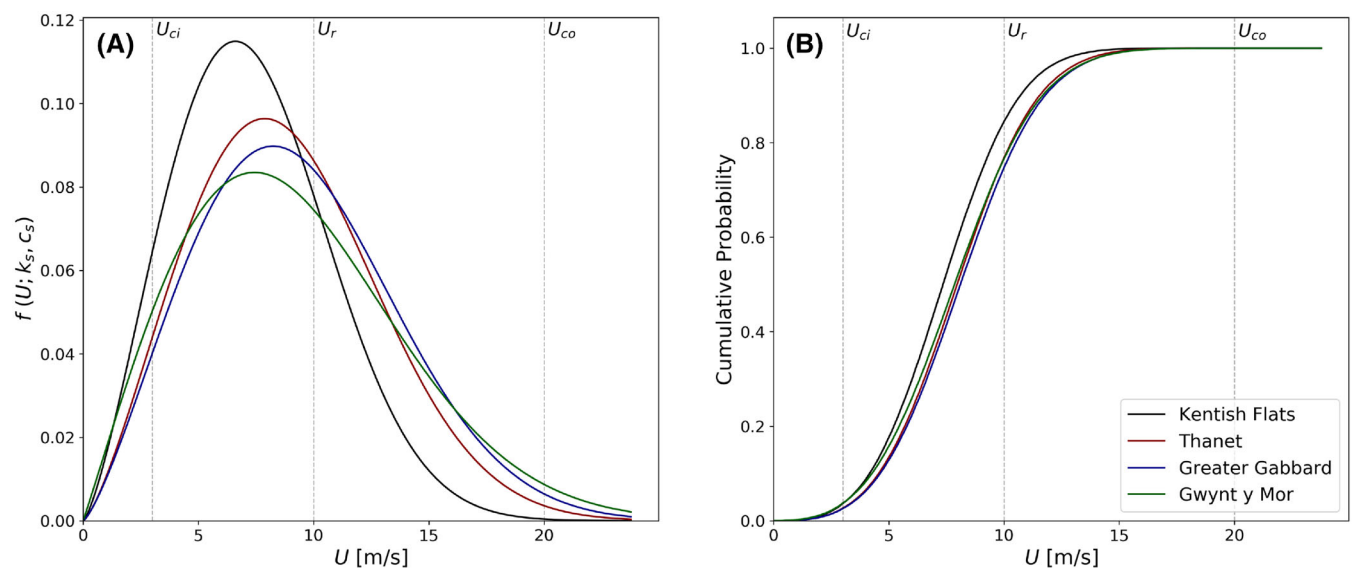


FIGURE 4 Wind speed probability distributions modelled with (A) the two parameter Weibull distribution and (B) the cumulative probability density for the Kentish Flats, Thanet, Greater Gabbard and Gwynt y Mor sites. Vertical lines have been added to indicate U_{ci} , U_r and U_{co} . Wind speed data are from 10-min average data extrapolated through a low law profile to a common altitude of 80 m

clean and rough airfoil data is provided in Table 4. C_T is defined analogously to the local thrust coefficient, as the ratio of rotor thrust, T , to the force generated by the upstream dynamic pressure acting on the frontal area of the turbine:

$$C_T = \frac{T}{(1/2)\rho U^2 A}. \quad (7)$$

In all cases, at the design point, the turbine power is adversely affected by blade roughness. This performance reduction is accompanied by a reduction in observed turbine thrust at this specific tip-speed-ratio.

3.2 | Turbine performance comparisons

Figure 5 illustrates the performance of the turbines with wind speed for clean and rough rotors using each of the control methods. On initial inspection, the torque-referenced control strategies (CM2 and 3) are more effective than the wind speed-controlled strategy (CM1), as indicated by the higher power they achieve relative to CM1 across all flow speeds. All roughened rotor cases achieve lower power than the clean rotor in below rated conditions highlighting the effect that airfoil roughness has on rotor torque.

For all control strategies, the clean airfoil turbines perform identically because the rotor is designed to operate with this airfoil, meaning that C_P and λ take optimal values for the clean rotor, and ω_r and τ_r occur at the same wind speed. The roughened airfoil rotors have cut-in speeds at higher wind speeds (3.2, 3.2 and 3.3 m/s for the NACA4415, S801 and S810 rotors, respectively) than the clean rotor, as a high wind speed is required to attain the same cut-in torque as in clean operating conditions.

Analysing CM1 between cut-in wind speed and rated flow speed, the roughened blade produces less power due to the reduction in torque (at a given rotational speed) that arises due to the reduced lift and increased drag of the roughened airfoils. The NACA4415 rotor has a maximum power (P^*) difference of 0.29 MW with the clean rotor producing $P_{clean}^* = 2.40$ MW. Similarly, the S801 rotor maximum power drops from $P_{clean}^* = 2.46$ MW to $P_{rough}^* = 2.20$ MW, and the S810 rotor maximum power drops from $P_{clean}^* = 2.37$ MW to $P_{rough}^* = 1.92$ MW. For all CM1 cases, both smooth and rough rotors reach maximum rotational speed at the rated wind speed, as stipulated by the control method. Consequently, both clean and roughened rotors start to pitch at a wind speed of 10.0 m/s, which also corresponds to the point of maximum thrust (T^*) for all rotors. For all rotors $T_{clean}^* = 407$ kN, as they are designed using the same design condition as discussed in Section 2.2. The roughened NACA4415 rotor has a peak thrust $T_{rough}^* = 371$ kN, while for the S801 rotor $T_{rough}^* = 364$ kN, and for the S810 rotor, $T_{rough}^* = 360$ kN.

Above rated speed, different trends between the clean and rough airfoil rotors emerge. The clean airfoil turbines adjust their blade root pitch angle to maintain rated power, giving rise to a 'typical' power curve. However, the roughened blade rotor has $\partial P_{CM1}/\partial U < 0$ above rated flow speed. This occurs because the pitching mechanism is designed to maintain generator torque for the clean airfoil and is thus suboptimal when the rotor aerodynamics have changed. The changed aerodynamics can be understood through Equations (8) and (9), where $C_t(\phi)$ is the tangential (torque-generating) component and $C_n(\phi)$ is the normal (thrust-generating) component of force on the rotor, respectively, where the flow incidence angle $\phi = \alpha + \beta_t$, where $\beta_t = \beta_g + \beta$ where β_g is the initial geometric twist of the blade and β is the additional blade pitch through control. The general trend of airfoil roughness is for lift to decrease and drag to increase, which results in $C_t(\phi)$ decreasing in all cases and $C_n(\phi)$ remaining approximately constant. Therefore, at a given α , the torque is reduced, and thrust is similar between clean and roughened cases.

$$C_t(\phi) = c_l(\alpha)\sin(\phi) - c_d(\alpha)\cos(\phi) \quad (8)$$

$$C_n(\phi) = c_l(\alpha)\cos(\phi) + c_d(\alpha)\sin(\phi) \quad (9)$$

TABLE 4 Coefficient of performance and thrust coefficient for each rotor operating under design conditions ($\lambda^* = 10$, $U_r = 10$ m/s) for clean and rough airfoil data

Rotor	Airfoil condition	C_P	C_T
NACA4415	Clean	0.4991	0.8540
NACA4415	Rough	0.4382	0.7784
S801	Clean	0.5107	0.8540
S801	Rough	0.4571	0.7647
S810	Clean	0.4932	0.8540
S810	Rough	0.3995	0.7567

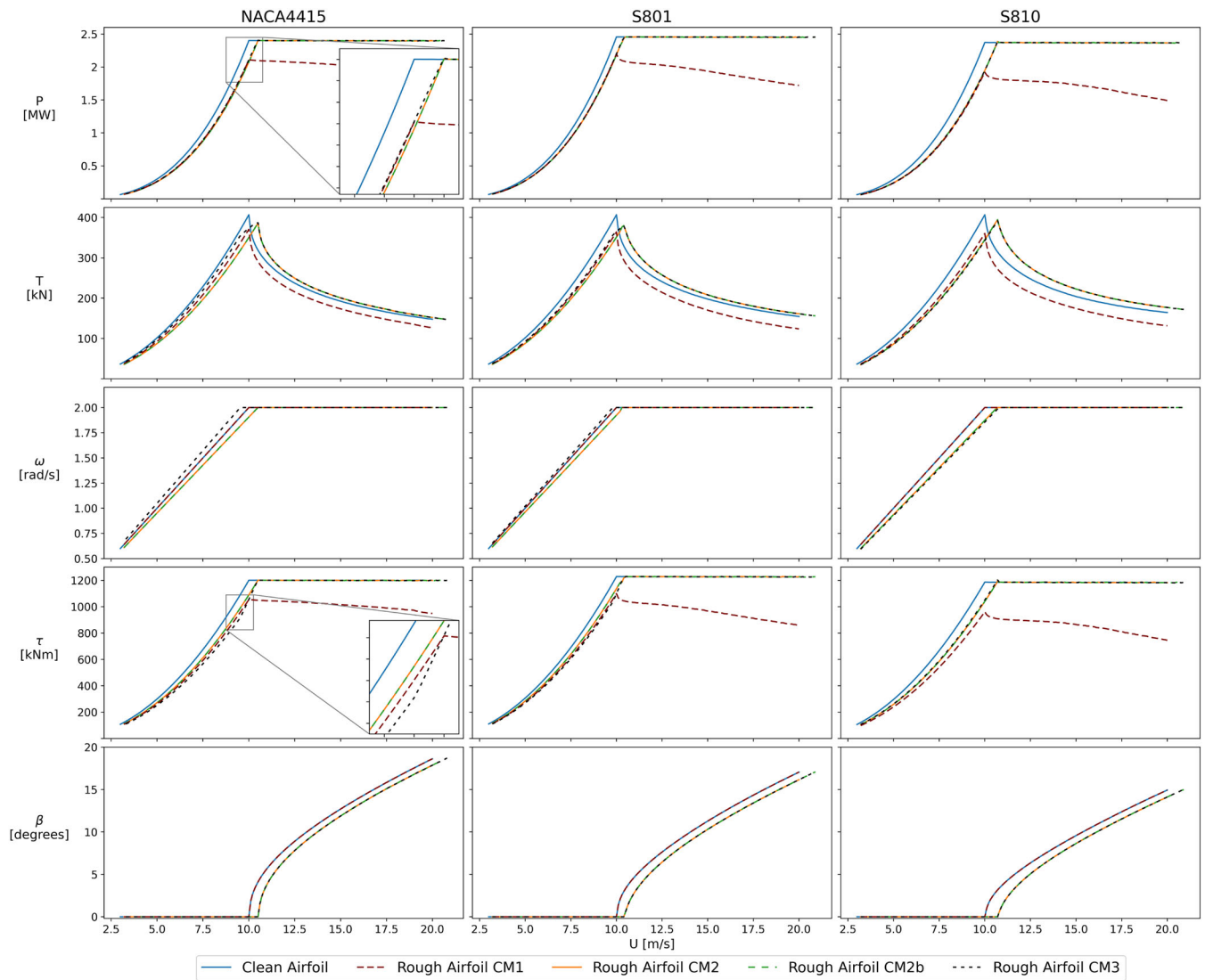


FIGURE 5 Performance comparison between rotors with roughened and clean blades for the three rotor designs (NACA4415 left, S801 centre, S810 right) for all control methods. The x-axis for all plots is wind speed. Two inset graphs are present: one for the NACA4415 power versus wind speed, which demonstrates the improved performance of CM3; and one for the NACA4415 torque versus wind speed, which illustrates the change in gradient for the CM3 torque profile in this area

Above rated flow speed, the blade pitch is adjusted to reduce α and thus reduce lift in order to limit rotor torque. Under CM1, this adjustment is performed at the same rate, as a function of wind speed, as for the clean rotor which, all other flow conditions being equal, produces more torque than a roughened rotor. Consequently, rotor torque and thus power slowly decrease with flow speed for the roughened rotor under CM1. This is highlighted in Figure 6 where torque reduces once the maximum rotational speed is achieved.

For the rough airfoil rotors, CM1 and CM2 perform similarly from cut-in wind speed to rated wind speed, as both control methods CM1 and CM2 utilise the same K_{clean} below rated. However, CM2 enables τ_{gen} to continue to increase beyond U_r until τ_r and P_r are reached. The rough airfoil turbine then pitches so as to maintain τ_r . For each of the clean rotors, rated power was reached at a wind speed of 10.0 m/s beyond which the blade pitch angle was adjusted to limit rotor power. Blade pitch adjustment doesn't occur until slightly higher flow speeds are reached for the rough rotors with pitching commencing once rated power is obtained at 10.5, 10.4 and 10.7 m/s for the NACA4415, S801 and S810 rotors, respectively. At the point that the roughened rotor with CM2 control reaches the cut-out speed, it has not obtained the maximum pitch setting β_{max} . The operating range of the roughened rotors can be extended using CM2b so that cut-out occurs at a higher wind speed once β_{max} is reached. The rotors cut out at wind speeds of 20.8, 20.9 and 20.9 m/s for the roughened NACA4415, S801 and S810 rotors, respectively, compared to a cut-out speed of 20 m/s for the clean rotors.

As may be inferred from Equations (2), (3) and (8), adjusting the turbine control to account for roughness may help increase rotor torque relative to control based on clean blade characteristics. This results in the different control curves in Figure 6, where increasing K reduces the curve

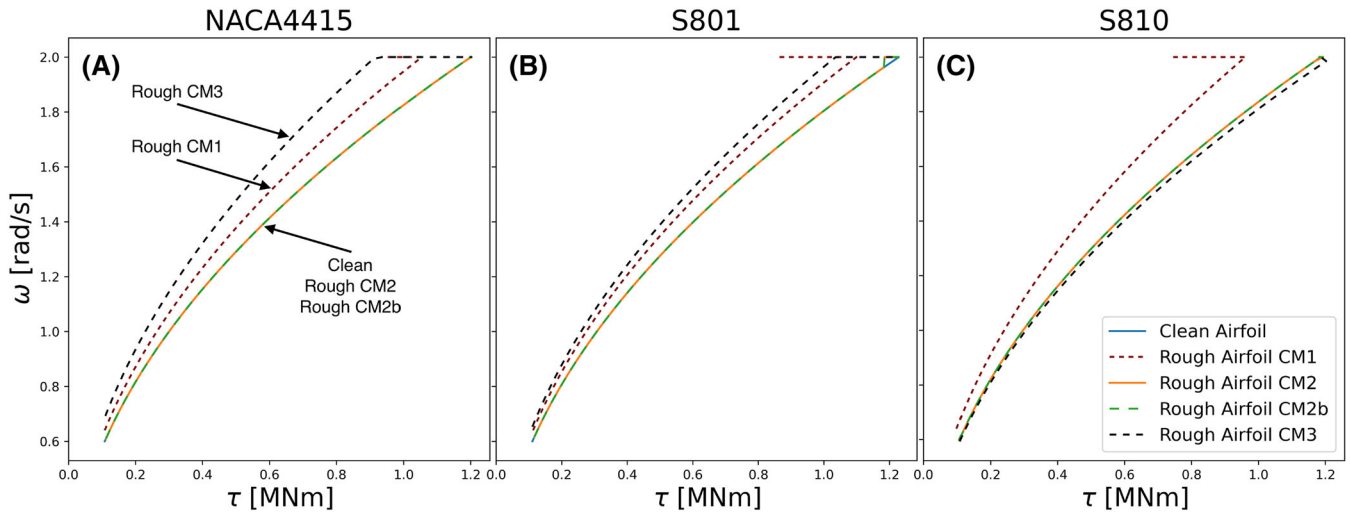


FIGURE 6 Torque as a function of rotational speed for the (A) NACA4415 rotor, (B) S801 rotor and (C) S810 rotor, for both clean and rough airfoil conditions and all control methods

gradient. CM3 adjusts this balance by determining a K value that maximises AEP based on the roughened airfoil characteristics. The power inset plot in Figure 5 shows the improved performance (higher power) for a given wind speed from using CM3 compared to CM2. Each rotor changes differently, as the different aerodynamic properties of the rotor airfoils result in the roughened rotor $C_p - \lambda$ power curve changing differently such that the required change to K to re-optimize for roughened performance can be by different magnitudes and in different directions. The purpose of changing K is to recover some of the power that is lost below rated torque due to erroneous control of the rotor as if it were still clean. Whether K_{rough} is greater or less than K_{clean} depends on the α required to achieve maximum rough c_l/c_d compared to that required to achieve the maximum in the clean condition.

It is useful to consider a representative angle of attack, $\bar{\alpha}$, to understand the direction K will move for a given airfoil rotor. When operating using K_{clean} (i.e., CM2/CM2b) with roughened blades, a range of α occurs along the span of the rotor (see Figure 8A) and $\bar{\alpha}$ can be thought of as being representative of these values. If $\alpha_{rough}^* > \bar{\alpha}$, then by increasing K , a lower rotational speed is prescribed, via Equation (3), resulting in an increase in the flow angle ϕ and therefore α , until $\bar{\alpha} \rightarrow \alpha_{rough}^*$ and a roughened rotor optimum is achieved. If initially $\alpha_{rough}^* < \bar{\alpha}$, then K must be decreased so as to recover the optimum. However, the exact required changes in K will be a function of blade twist distribution and are therefore too complex to define simply.

K is observed to increase for the S810 airfoil and decreases for the other two when optimised for roughness. These changes in K correspondingly decrease the rotational speed and therefore tip-speed ratio for S810 and increase these for the other rotors. By changing K , operational $C_{p, rough}$ is maximised from cut-in wind speed to rated torque. The cut-in flow speed also occurs approximately 0.1–0.2 m/s earlier with K optimised than with CM2/CM2b, as the required cut-in torque, τ_{ci} , is achieved for a lower wind speed with the optimised settings.

For CM3, as the flow speed is increased, the rotor spins more quickly than it would under CM2 and reaches maximum rotational speed, ω_r , ahead of obtaining maximum torque τ_r so that between the point of maximum ω and τ , the torque must rise rapidly with flow speed, and hence, $\partial\tau/\partial\omega$ increases as seen in the torque inset plot of Figure 5. This can be identified in the torque versus rotational speed plot for this case (Figure 6), which shows that once $\omega = \omega_r$, $\partial\omega/\partial\tau = 0$ as torque increases to its maximum value.

3.3 | Spanwise effects of roughness

Figure 7A shows the spanwise contribution to AEP along the rotor using CM2/CM2b and evaluated for the turbines using the Kentish Flats wind distribution. The shape of these distributions differs from the optimal performance torque profiles which increase monotonically to maxima at $r/R = 0.865$ for all rotors (both clean and rough) before tip loss effects cause the blade loads to reduce (see Figure 7B). Maximum torque occurs at the same radius for clean and rough rotors, whereas the radial location for maximum AEP contribution may shift inboard due to the influence of roughness. The change in peak torque per unit span produced between clean and rough blades is 10.9–18.6%, whereas the change in total AEP is 4.9–8.6% (based on the Kentish Flats wind distribution). Hence, we note that a combination of both roughness and wind speed characteristics are important for calculating performance losses. Figure 7A identifies that there is a fundamental performance difference between the S810 rotor and the NACA4415 and S801 rotors, especially over the inboard 50% of span. The differences in AEP distributions between the rotors arise as a result of the differences in torque generated by the different rotors and control methods.

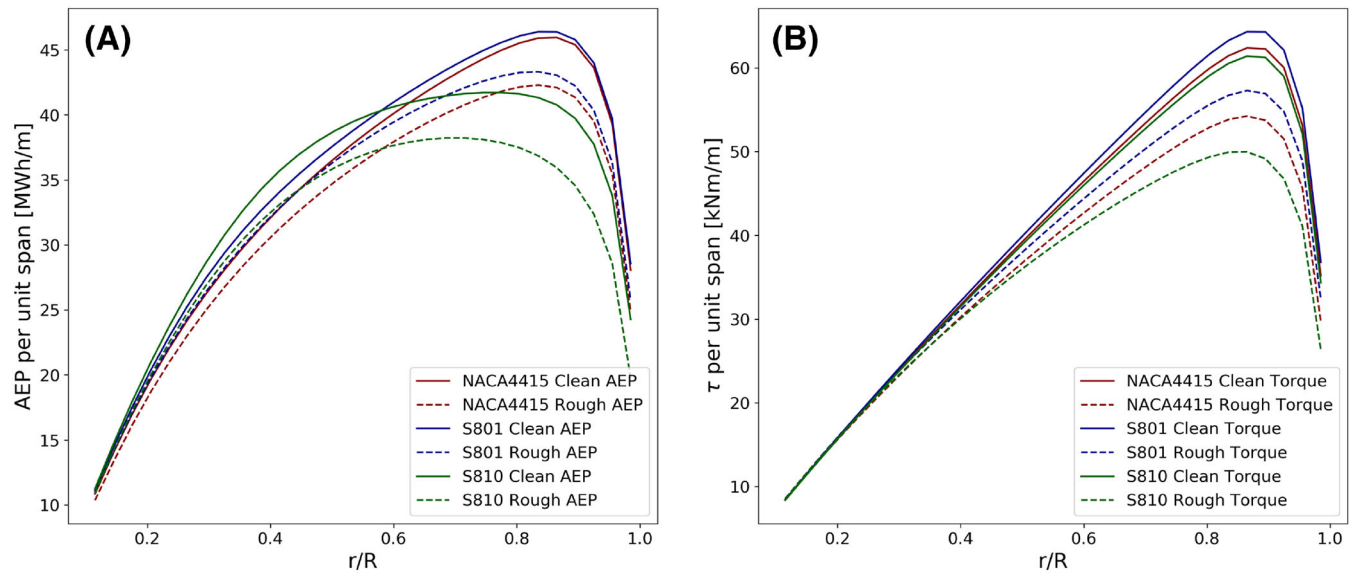


FIGURE 7 Spanwise variation of (A) AEP (evaluated for the Kentish Flats wind distribution) and (B) blade torque for the NACA4415, S801 and S810 rotors in clean and rough conditions using CM2/CM2b

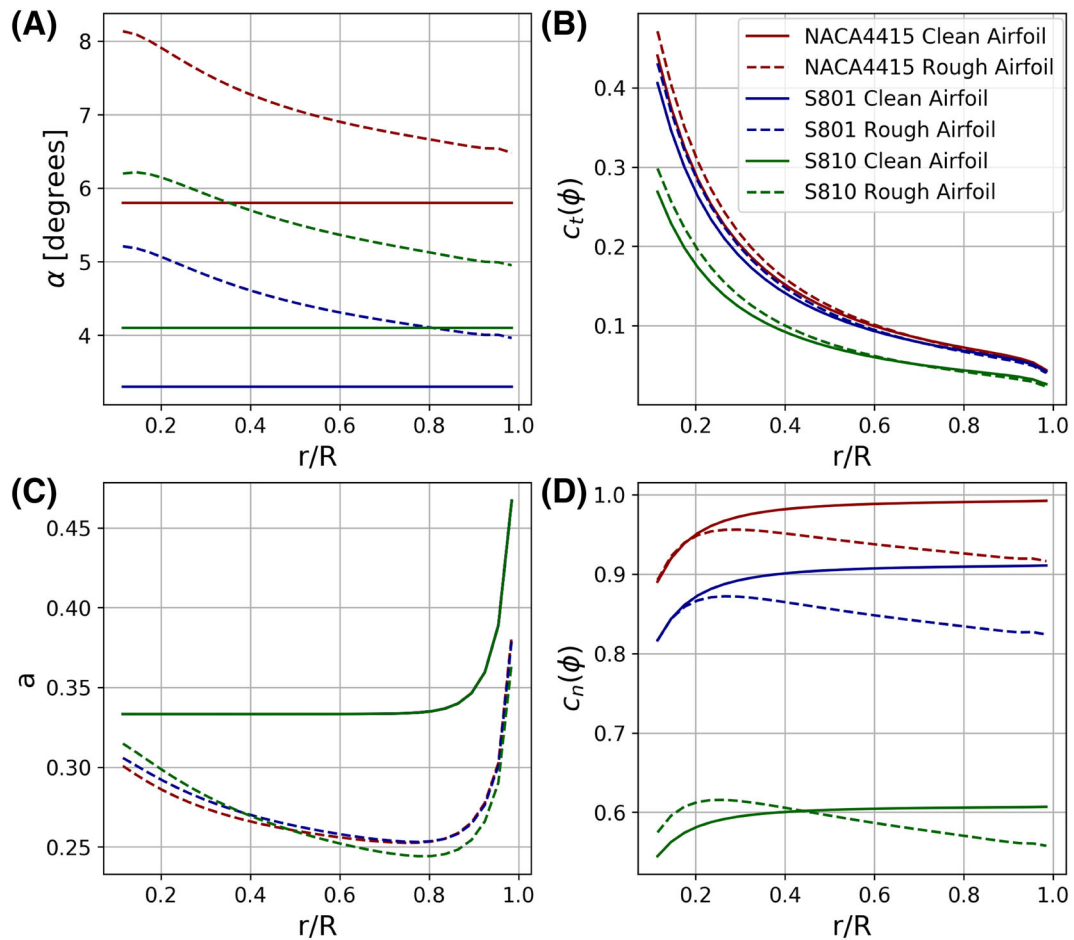


FIGURE 8 Spanwise analysis of NACA4415, S801, S810 rotors using CM2/CM2b for a wind speed of 10 m/s showing the spanwise variation of (A) angle of attack, α , (B) tangential force coefficient, $C_t(\phi)$, (C) axial induction factor, a and (D) normal force coefficient, $C_n(\phi)$

Figure 8 shows the differences in performance characteristics due to roughness for all investigated blades in their optimal operating state (below rated torque) for CM2/CM2b. The clean rotors all have a spanwise-constant angle of attack, α , and axial induction factor, a , as these are specified through the rotor design process; see Section 2.2 ($\alpha = \alpha^*$, $C_x = 2$). A consequence of rotor roughness is a reduction in rotational speed at any given pre-rated flow speed (see Figure 5), such that the roughened rotors operate at a lower tip-speed-ratio than λ_{clean}^* . This together with the reduction in airfoil forces due to roughness results in a reduction in thrust along the length of each blade; see Figure 8D, which results in an increase in axial flow speed through each turbine (reduction in induction factor a). Consequently, we observe a small increase in the angle of attack on the roughened blades. The increase in α , however, does not typically have a dramatic effect on the average operational lift-to-drag ratio value of each airfoil, shown in Table 5, other than the rough NACA4415 rotor. The greatest changes due to roughness can be seen in the normal and tangential force component plots, calculated using Equations (8) and (9), respectively.

Furthermore, a simple control strategy for a roughened turbine to optimise α at the angle of attack to achieve $(c_l/c_d)_{rough}^*$ will not produce optimal performance, because α_{rough}^* cannot be simultaneously achieved at all points along the rotor span. This is a consequence of the rotor being designed to operate with a clean airfoil at α_{clean}^* , and thus when roughness alters the aerodynamics, even if these changes are known, α^* cannot be produced along the entire span of the blade as $\alpha_{clean}^* \neq \alpha_{rough}^*$.

The performance differences in $C_t(\phi)$ and $C_n(\phi)$ between clean and rough conditions are a result of the changes in lift and drag airfoil characteristics and through a change in the operating point of the rotor (λ) under CM2/CM2b. It might be expected that roughness should lead to a reduction in tangential force at all spanwise locations. However, together with the change in tip-speed-ratio, the tangential force is observed to decrease across outboard sections but increase through inboard sections with a net resultant decrease in rotor torque due to roughness. Focusing on the operational airfoil characteristics in Table 5, the lift-to-drag ratio 'ranking' (from highest to lowest values), for the airfoils, corresponds to the performance order of the corresponding wind turbines for all wind sites.

3.4 | Roughness effects on airfoils

Figure 9 shows the lift and drag profiles in the angle of attack range encountered in turbine operation $0^\circ < \alpha < 10^\circ$, giving an indication of the effect of roughness on airfoil performance. Drag is approximately linear in this range and roughly doubles due to the effect of roughness for all airfoils. The increase in angle of attack that occurs when the airfoil is roughened (Figure 8A) results in a similar magnitude of the lift force in the pre-stall region between the clean and rough case (approximate reduction of 5%). Consequently, the change in drag is the primary factor in determining the reduction in operational lift-to-drag ratio and the magnitude of performance loss.

Figure 9C highlights the range of operational α and c_l/c_d values that occur between 40% and 100% span in clean and rough conditions below rated power. When the clean rotor operates in its design conditions, achieving a constant α that maximises c_l/c_d along the blade span. However, when blade roughness develops, the rotor no longer operates in design conditions, and consequently, the blade forces and the angle of attack will vary along the blade (see Figure 8A). The operational angle of attack increases when airfoil roughness develops, as highlighted in Figure 9C. The figure also shows that operating the roughened rotor as if it were clean (CM2) tends to miss the c_l/c_d peak of the roughened airfoil. Adjusting turbine control to account for the degraded aerodynamic characteristics of the airfoil (CM3) allows some performance to be recovered by adjusting rotor speed to ensure that the operating α range of the rotor under CM3 encompasses the roughened airfoil c_l/c_d peak. This process is highlighted for the NACA4415 airfoil in Figure 10, with arrows included to indicate the impact of blade degradation (c_l/c_d decreased by c. 56%) and the performance recovery impact of changing from CM2 to CM3 (average c_l/c_d increased by c. 18%).

The increase in drag results in a decrease of the rough airfoil lift-to-drag ratio and attendant reduction in the slope of the lift-to-drag curve $d(c_l/c_d)/d\alpha$. Therefore, even if the rotor does not achieve the optimal roughened angle of attack along the blades, $d(c_l/c_d)/d\alpha$ is small so that the rotor is found to operate close to, but not at, its maximum possible efficiency. The roughened performance can therefore only be marginally improved by further changing α . Consequently, while it is possible to alter K in CM3, only small improvements in power will result for the rotors

TABLE 5 The maximum lift-to-drag ratios for NACA4415, S801 and S810 airfoils, together with the spanwise-averaged rotor lift-to-drag ratios for operation using CM2/CM2b

Rotor	Airfoil condition	Maximum c_l/c_d at α^*	Spanwise average c_l/c_d
NACA4415	Clean	102.45	102.45
NACA4415	Rough	52.64	44.86
S801	Clean	129.75	129.75
S801	Rough	60.50	60.33
S810	Clean	92.62	92.62
S810	Rough	36.84	36.59

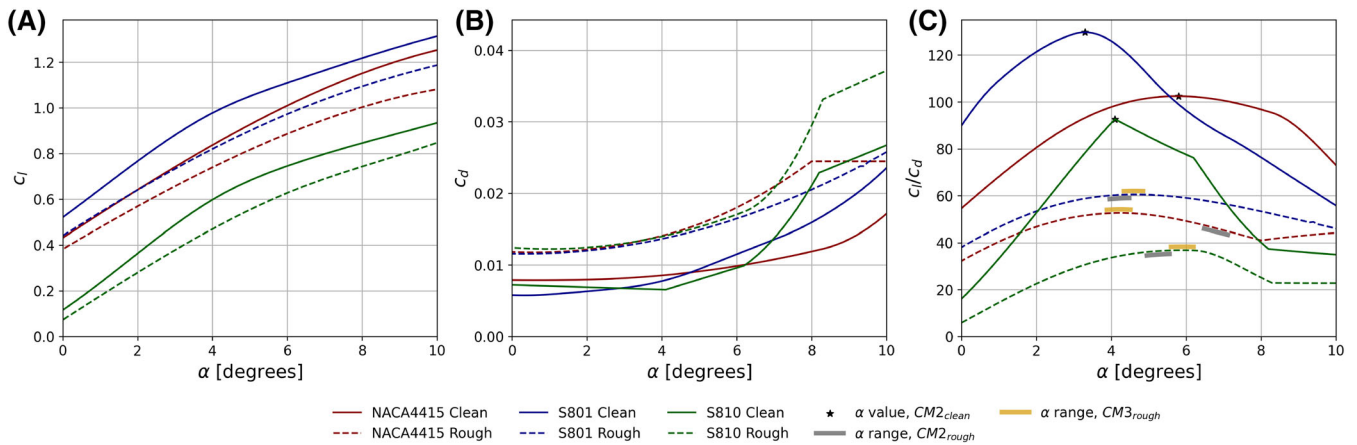


FIGURE 9 Airfoil characteristics c_l (A), c_d (B) and c_l/c_d (C) in the angle of attack region most relevant to turbine operation, $0^\circ < \alpha < 10^\circ$ for NACA4415, S801 and S810 airfoils. The operational α values (40–100% span) for the different control strategies have been highlighted, with all clean cases denoted CM_{clean}

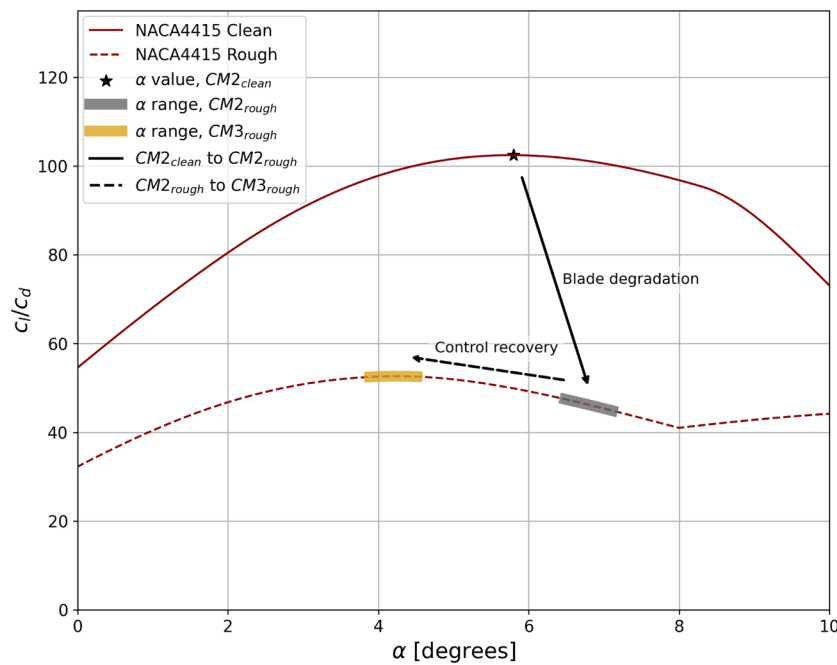


FIGURE 10 Airfoil characteristics c_l/c_d in the angle of attack region most relevant to turbine operation, $0^\circ < \alpha < 10^\circ$ for the NACA4415 airfoil. The operational α values (40–100% span) for the different control strategies have been highlighted, with clean cases denoted CM_{clean} and rough cases denoted CM_{rough} . Arrows indicate the impact of roughness and the control recovery mechanism of CM3

studied herein and for the given levels of roughness. It is therefore of interest to ensure that airfoils used in wind turbine applications maintain a high lift coefficient and limited increase in drag due to roughness.

3.5 | Energy loss

The impact of roughness on energy production based on the wind distributions identified in Table 3 is shown in Figure 11. For all rotors, performance under CM1, where the turbine control is effectively referenced to a measured wind speed, is worst and results in very undesirable reductions in performance of up to around 20%. For the torque-based CM2 control method in which the pre-rating control (K value) remains unaltered, the performance reduction ranges between 2% and 8% depending on the rotor and site, with the S801 rotor showing least sensitivity in AEP to roughness, and the S810 rotor showing the greatest losses. For all rotors and sites, some AEP may be recovered through control method CM2b

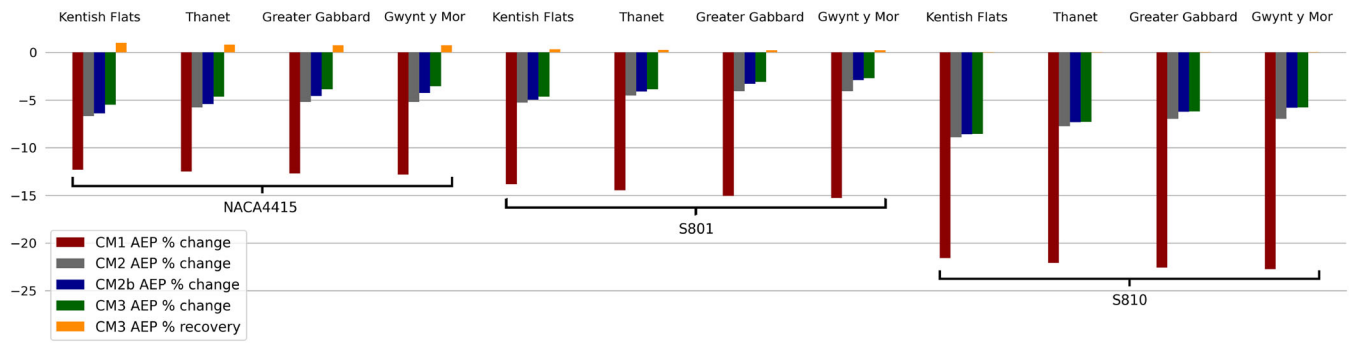


FIGURE 11 Energy capture comparison between clean and rough rotors operated with different control methods over a 1-year time period. AEP changes are measured relative to the clean operating rotor, and CM3 recovery is measured relative to CM2b

which extends the cut-out speed to higher flow speeds so that the maximum pitch angle β_{max} reached under rough airfoil conditions is the same as that reached at cut-out for the clean rotor. By altering the pre-rated control coefficient to K_{rough} , CM3 is able to achieve a partial yield recovery relative to CM2b, with a smaller performance drop relative to the clean rotors. The recovery in AEP from CM2b to CM3 across the sites is between 0.73% and 0.98%, 0.22% and 0.31% and 0.04% and 0.05% for the NACA4415, S801 and S810 airfoil rotors, respectively (Figure 11).

The possibility for partial power recovery through this simple controller-based mechanism is demonstrated to be achievable but limited in scope due to the underlying performance reduction of the airfoils due to roughness; the approximate doubling of drag imposes an unrecoverable negative impact on rotor torque. However, this is a relatively simple adjustment of rotor operation and therefore may still be an attractive method for mitigating performance loss, and thus recovering some energy yield, previously lost due to roughness. We note that the impact that roughness has on turbine lifetime due to increased unsteady loading may also be significant but cannot presently be estimated with a steady-state model such as BEM theory and the available airfoil data.

The S810 rotor performs notably worse than the other two rotors presented herein. The S810 airfoil produces significantly less lift (clean or rough) than the other airfoils considered in this study, whereas its drag is similar. This is a function of the lower design max c_l for this airfoil, as highlighted in Table 1. Consequently, a large blade chord was required (see Figure 2) to meet the design requirements (thrust level), which also results in a greater contribution towards overall rotor AEP from the inboard portions of the blade (see Figure 7A).

The varying ranges of performance losses shown in Figure 11 indicate the effect of wind distribution on the impact of roughness. The greater the likelihood of wind speeds above the rated speed (shown in Figure 4 and Table 3), the more likely the turbine is to operate at the rated power, whether clean or rough, thus reducing the negative effect of roughness on overall energy production. Figure 4 shows that the Kentish Flats site has the greatest probability of wind speeds below U_r , which gives rise to the largest performance decline from roughness. In effect, roughness only affects turbine performance when operating between P_{ci} and P_r , noting that roughness can cause a change in the wind speed at which P_r is achieved. Similarly, CM3 is only able to improve power production in this range, so as the percentage change in performance due to roughness decreases, so does the percentage improvement from using CM3.

4 | CONCLUSIONS

This study has explored the effect on wind turbine performance and AEP when operating with full-spanwise roughened rotor blades. Experimental data from three NREL-tested airfoils were used to provide clean and rough aerodynamic lift and drag data. The clean airfoil data were used with an in-house BEM design tool to develop clean rotor blade designs that sought to operate at a design angle of attack along the blade and a prescribed local thrust coefficient.

The in-house BEM tool was used for clean operation and for roughened rotor operation considering three control methods: turbine operation referenced to wind speed (CM1); turbine operation referenced to generator torque (CM2); and a K -optimised torque control method for energy yield recovery (CM3). CM1 provided a baseline for comparison by adjusting the rotor speed and blade pitch angle with wind speed in the same manner as for each of the clean wind turbines. The rough airfoil rotors were unable to achieve rated torque and energy losses ranged from 12.4% to 22.8% across four different candidate wind sites considered.

In CM2, the rotor seeks to balance aerodynamic and generator torque below rated torque by adjusting rotational speed and above rated torque by pitch-to-feather control. Roughness leads to a slower rotational speed before rated torque is reached, with rated torque itself delayed to a higher flow speed than for the clean rotors. CM2 was found to be more effective than CM1, with energy losses ranging from 3.3% to 8.6% across the three rotors and four sites considered. A slight increase in energy yield was found using CM2b which extended the cut-out speed to higher

flow speeds such that the maximum blade pitching of the roughened rotor blades matched that of the clean rotors at cut-out. CM3 improved on CM2 by optimising the controller gain parameter K for operating the rough rotors. The required change in K from clean to rough conditions is found to be dependent on rotor geometry and the change in airfoil performance characteristics between clean and rough conditions. The rough rotors are found to produce highest energy yield using CM3, which reduces energy losses by a further 0.1–1.0% relative to CM2b.

A significant performance drop was found for all simulated control strategies across the representative sites considered in this study. Using four separate wind farm sites for wind speed distributions, yearly energy losses between 2.9% and 8.6% were found for the three rotors using CM2/CM2b. CM3 was able to ‘recover’ some portion, up to about 1%, of the power lost through re-optimising K . This re-optimisation adjusts the rotational speed of the rotor below rated torque to account for roughness effects. This is a simple control-based energy yield recovery strategy. The extent to which energy yield recovery can be achieved is limited due to the high increase in blade drag through roughness and the resulting reduction in the rate of change of the lift-to-drag ratio with angle of attack. Further research is required to identify airfoils and rotor designs that are less sensitive to the development of blade roughness.

ACKNOWLEDGEMENTS

The authors would like to acknowledge The Australia Day Foundation UK Trust for their support for JK in conducting this study and EPSRC who support RW's research through an EPSRC Advanced Fellowship EP/R007322/1 and the EPSRC Supergen ORE Hub, grant number EP/S000747/1.

PEER REVIEW

The peer review history for this article is available at <https://publons.com/publon/10.1002/we.2691>.

DATA AVAILABILITY STATEMENT

The data that support the findings of this study are openly available at <https://www.nrel.gov/wind/nwtc/airfoils-osu-data.html>, reference number [23].

ORCID

Jack Kelly  <https://orcid.org/0000-0002-0501-4650>

Christopher Vogel  <https://orcid.org/0000-0003-2232-9811>

REFERENCES

1. Corten GP, Veldkamp HF. Insects can halve wind-turbine power. *Nature*. 2001;412(6842):41–42.
2. Jasinski WJ, Noe SC, Selig MS, Bragg MB. Wind turbine performance under icing conditions. *Solar Energy Eng*. 1998;120(1):60–65.
3. Corrigan RD, DeMiglio RD. Effect of precipitation on wind turbine performance. Report No NASA-TM-86986, National Aeronautics and Space Administration Report. Springfield, VA; 1985.
4. Khalfallah MG, Koliub AM. Effect of dust on the performance of wind turbines. *Desalination*. 2007;209(1-3):209–220.
5. Blasco P, Palacios J, Schmitz S. Effect of icing roughness on wind turbine power production. *Wind Energy*. 2017;20(4):601–617.
6. Brandrud L, Krøgenes J. Aerodynamic performance of the NREL S826 airfoil in icing conditions. *Master's Thesis: NREL S826 Airfoil in Icing Conditions*; 2017.
7. Hann R, Hearst RJ, Sætran LR, Bracchi T. Experimental and numerical icing penalties of an S826 airfoil at low Reynolds numbers. *Aerospace*. 2020;7(4):46.
8. Vinnes MK, Hearst RJ. Aerodynamics of an airfoil with leading-edge icing. *Wind Energy*. 2020;24(8):795–811.
9. De Gregorio F, Ragni A, Airolidi M, Romano GP. PIV investigation on airfoil with ice accretions and resulting performance degradation. In: ICIASF 2001 record, 19th international congress on instrumentation in aerospace simulation facilities (cat. no. 01ch37215). Cleveland, OH; 2001:94–105.
10. Janiszewska JM, Ramsay RR, Hoffmann MJ, Gregorek GM. Effects of grit roughness and pitch oscillations on the S814 airfoil. tech. rep., Golden, CO (United States), National Renewable Energy Lab.; 1996.
11. Sareen A, Sapre CA, Selig MS. Effects of leading edge erosion on wind turbine blade performance. *Wind Energy*. 2014;17(10):1531–1542.
12. Schmitz S. Xturb-psu: A wind turbine design and analysis tool. *The Pennsylvania State University*. 2012.
13. Krog Kruse E, Sørensen NN, Bak C. A two-dimensional quantitative parametric investigation of simplified surface imperfections on the aerodynamic characteristics of a NACA 63₃-418 airfoil. *Wind Energy*. 2021;24(4):310–322.
14. Munduate X, Ferrer E. CFD predictions of transition and distributed roughness over a wind turbine airfoil. In: 47th AIAA Aerospace Sciences Meeting including The New Horizons Forum and Aerospace Exposition. Orlando, FL; 2009:269.
15. Schramm M, Rahimi H, Stoevesandt B, Tangager K. The influence of eroded blades on wind turbine performance using numerical simulations. *Energies*. 2017;10(9):1420.
16. Jonkman J. Fast. Wind Research | NREL, date accessed 05/12/2019, available at <https://www.nrel.gov/wind/nwtc/fast.html>
17. Pechlivanoglou G, Fuehr S, Nayeri CN, Paschereit CO. The Effect of Distributed Roughness on the Power Performance of Wind Turbines. Volume 5: Industrial and Cogeneration; Microturbines and Small Turbomachinery; Oil and Gas Applications; Wind Turbine Technology; 2010.
18. Hansen MOL. *Aerodynamics of Wind Turbines*. London: Routledge; 2015.
19. Bak C, Forsting AM, Sorensen NN. The influence of leading edge roughness, rotor control and wind climate on the loss in energy production. *J Phys*. 2020;1618(5):052050.

20. Hasager CB, Bech JJ, Bak C. On leading edge erosion at turbine blades due to heavy rain and the application of erosion safe mode control to extend life. In: 3rd ACI operations & maintenance for offshore wind. Copenhagen, Denmark; 2019.
21. Tilg A-M, Hasager CB, Kirtzel H-J, Hummelshøj P. Brief communication: nowcasting of precipitation for leading-edge-erosion-safe mode. *Wind Energy Sci.* 2020;5(3):977-981.
22. Hasager CB, Vejen F, Skrzypiński WR, Tilg A-M. Rain erosion load and its effect on leading-edge lifetime and potential of erosion-safe mode at wind turbines in the North Sea and Baltic Sea. *Energies.* 2021;14(7):1959.
23. Buhl ML. Ohio State University Wind Tunnel Tests. NREL Wind Research, date accessed 01/10/2019, available at <https://www.nrel.gov/wind/nwtc/airfoils-osu-data.html>
24. Ning SA. A simple solution method for the blade element momentum equations with guaranteed convergence. *Wind Energy.* 2014;17(9):1327-1345.
25. Prandtl L, Betz A. *Vier Abhandlungen zur Hydrodynamik und Aerodynamik.* Göttingen: Universitätsverlag Göttingen; 1927.
26. Buhl ML. New Empirical Relationship between Thrust Coefficient and Induction Factor for the Turbulent Windmill State. Technical Report NREL/TP-500-36834. Golden, CO: National Renewable Energy Laboratory (NREL); 2005.
27. Vogel CR, Willden RHJ, Houlby GT. Blade element momentum theory for a tidal turbine. *Ocean Eng.* 2018;169:215-226.
28. Buhl ML. Wind turbine airfoils, NREL—National Renewable Energy Laboratory, NWTCT Information Portal, date accessed 01/10/2019, available at <https://wind.nrel.gov/airfoils/Documents/AirfoilDocuments.html>
29. Hoffmann MJ, Reuss Ramsay R, Gregorek GM. Effects of grit roughness and pitch oscillations on the NACA 4415 airfoil. NREL/TP-442-7815, Columbus, OH (United States); 1996.
30. Tangler JL, Somers DM. NREL airfoil families for HAWTs. tech. rep., Golden, CO (United States), National Renewable Energy Lab.; 1995.
31. Reuss Ramsay R, Hoffmann MJ, Gregorek GM. Effects of grit roughness and pitch oscillations on the S801 airfoil. NREL/TP-442-7818, Columbus, OH (United States), National Renewable Energy Lab., Golden, CO (United States); The Ohio State Univ.; 1996.
32. Reuss Ramsay R, Hoffmann MJ, Gregorek GM. Effects of grit roughness and pitch oscillations on the S810 airfoil. NREL/TP-442-7816, Columbus, OH (United States), National Renewable Energy Lab., Golden, CO (United States); The Ohio State Univ.; 1996.
33. Vestas. V120-2.2 MWTM. available at https://www.vestas.com/en/products/2-mw-platform/v120-22_mw#!. Date accessed 20/09/2019.
34. Siemens Gamesa Onshore Wind Turbine SG 2.6-114. available at <https://www.siemensgamesa.com/en-int/products-and-services/onshore/wind-turbine-sg-2-6-114>. Date accessed 20/09/2019.
35. Manwell JF, McGowan JG, Rogers AL. *Wind Energy Explained: Theory, Design and Application.* Chichester: John Wiley & Sons; 2010.
36. Jonkman J, Butterfield S, Musial W, Scott G. Definition of a 5-MW Reference Wind Turbine for Offshore System Development. Technical Report NREL/TP-500-38060. Wiley, Chichester, UK; 2009.
37. Burton T, Jenkins N, Sharpe D, Bossanyi E. *Wind Energy Handbook.* Chichester: John Wiley & Sons; 2011.
38. Menezes EJM, Araújo AM, da Silva NSB. A review on wind turbine control and its associated methods. *Journal of Cleaner Production.* 2018;174:945-953.
39. Fréchet M. Sur la loi de probabilité de l'écart maximum. *Ann Soc Polon Math.* 1927;6:93-116.
40. The Crown Estate. Wind Data, The Crown Estate - Marine Data Exchange, date accessed 08/08/2019, available at <http://www.marinedataexchange.co.uk/wind-data.aspx>
41. Bañuelos-Ruedas F, Angeles-Camacho C, Rios-Marcuella S. Analysis and validation of the methodology used in the extrapolation of wind speed data at different heights. *Renew Sustain Energy Rev.* 2010;14(8):2383-2391.
42. Wieringa J. Updating the Davenport roughness classification. *J Wind Eng Industr Aerodyn.* 1992;41(1-3):357-368.

How to cite this article: Kelly J, Vogel C, Willden R. Impact and mitigation of blade surface roughness effects on wind turbine performance. *Wind Energy.* 2021;1-18. doi:10.1002/we.2691